International Journal of Biological Macromolecules 168 (2021) 792–805

Contents lists available at ScienceDirect

International Journal of Biological Macromolecules

journal homepage: http://www.elsevier.com/locate/ijbiomac

Fractionation of lignin using organic solvents: A combined experimental and theoretical study

Veerapandian Ponnuchamy [a,c,*,1], Oihana Gordobil [a,**,1], René Herrera Diaz [a,d], Anna Sandak [a,b], Jakub Sandak [a,c]

[a] InnoRenew CoE, Livade 6, 6310 Izola, Slovenia
[b] University of Primorska, Faculty of Mathematics, Natural Sciences and Information Technologies, Glagoljaška 8, 6000 Koper, Slovenia
[c] University of Primorska, Andrej Marušič Institute, Titov trg 4, 6000 Koper, Slovenia
[d] Chemical and Environmental Engineering Department, University of the Basque Country, San Sebastian, Spain

ARTICLE INFO

Article history:
Received 7 October 2020
Received in revised form 8 November 2020
Accepted 20 November 2020
Available online 23 November 2020

Keywords:
Hardwood kraft lignin
Fractionation
Chemometrics
Density functional theory
Hydrogen bonds
Noncovalent interactions

ABSTRACT

Refining of industrial lignin to produce homogeneous fractions is essential for high-value applications. However, the understanding of key interactions between a variety of solvents with lignin polymer is still uncertain. In this work, single-step fractionation of industrial hardwood kraft lignin (HKL) using organic solvents of different polarities – ethanol, acetone, diethyl ether and hexane – was investigated by combining an experimental and theoretical approach. Experimental results revealed that higher polarity solvents (ethanol and acetone) exhibited higher solubility yield compared to moderate and low polarity solvents. The chemical differences between lignin fractions were proven by pyrolysis gas chromatography mass spectrometry and near infrared spectroscopy. Density functional theory (DFT) results indicated that ethanol presented higher interaction energy followed by acetone, diethyl ether and hexane, which was consistent with experimental findings. Hydrogen bond and noncovalent interaction results from DFT demonstrated that the predominant interaction was found for high polarity of ethanol over other solvents and γ-OH in the lignin model is the key site.

1. Introduction

Reduction and revalorization of industrial by-products is an environmental and social challenge. Kraft pulping process is the standard method for delignification of wood to convert it to paper pulp. This industrial process annually produces a large kraft lignin-rich residual stream that is typically combusted, resulting in low-value utilization [1]. Therefore, from the industrial point of view, recovery and valorization of kraft lignin for high-value applications, aside from supporting circular bioeconomy policy, could also be the trigger for further development of biorefineries in the near future [2,3].

The lignin polymer's complex chemical structure has been the subject of many studies over the years. However, it is still difficult to understand lignin chemistry and structure-properties relationships. This industrial waste has revealed high potential for numerous applications, and over the years, kraft lignin has been evaluated as a renewable source for the production of fine chemicals and gaseous products through thermochemical and biochemical methods [4,5]. Moreover, several efforts have been made to incorporate kraft lignin into the polymeric industry both as an additive in natural and synthetic polymers [6,7] and as precursor to synthesize various target applications including polyurethanes, phenol-formaldehyde and epoxy resins, energy harvesting and storage, carbon-fibre and filler in composites [8–12]. New applications are emerging for lignin polymer and lignin-derived products in different fields. For example, lignin-based products are becoming attractive materials for pharmacological and biomedical applications. Research is focused on the evaluation of lignin's bioactive properties such as its anti-tumour, antiviral, anti-diabetic, antioxidant and antimicrobial activities [13–15]. Development of drug delivery systems and functional materials for tissue engineering, based on lignin, is also a topic of great interest [13,16]. In addition, consideration of lignin polymer as a sunscreen agent for cosmetics and health care products is growing [17].

Despite the high application potential of this abundant aromatic compound, industrial valorization of kraft lignin is highly restricted by its heterogeneous structural features, which cause undesirable properties for particular applications. To date, several studies have been conducted to overcome this problem. The fractionation of lignin using organic solvents, described for the first time in the 1980s by Mörck and coworkers [18], has been demonstrated to be an efficient method to improve lignin homogeneity and reduce its complexity. For this

* Correspondence to: V. Ponnuchamy, University of Primorska, Andrej Marušič Institute, Titov trg 4, 6000 Koper, Slovenia.
** Corresponding author.
E-mail addresses: veerapandian.ponnuchamy@innorenew.eu (V. Ponnuchamy), oihana.gordobil@innorenew.eu (O. Gordobil).
[1] These authors have equally contributed to this work

https://doi.org/10.1016/j.ijbiomac.2020.11.139

purpose, a wide range of organic solvents has been evaluated such as alcohols, ketones, esters, ethers, chlorinated solvents and alkenes [19–23]. Most of the reported work has centered on development of an effective fractionation process and elucidation of the structural and thermal properties of isolated lignin fraction.

The available literature evidence that the solubilization yield of lignin in organic solvents depends largely on the chemical nature of the solvent. However, the yield is also highly influenced by the lignin source and its structural characteristics, like molecular mass, monomeric composition and chemical functionality [24–26]. Solubilization yield and molecular weight of isolated lignin fractions increase with increase of the hydrogen bonding capacity and polarity of the solvents, while low molecular mass fractions are usually associated with low extraction yields and weak hydrogen bonding capacity and low polarity of the solvent [24,27–29]. Passoni et al. [30] reported that the solubility of lignin in a given solvent is correlated to its ability to establish different intermolecular interactions with aliphatic, carbonyl and hydroxyl groups of the lignin structure.

However, how is lignin-solvent interaction mechanism? What are the active sites that make lignin solubilize? Despite numerous research works related to lignin fractionation using organic solvents, these questions have not yet been explained. In this work, combined experimental and theoretical study was carried out with the aim to fractionate industrial lignin and answer unknown aspects related to lignin-solvents interaction mechanism.

In addition to the experiments, quantum chemical density functional theory (DFT) calculations provide significant insight to understand and evaluate the fundamental interaction involved in the system containing lignin with different solvents. Because the complex structure of lignin, considering a structure with all linkages present in the lignin would be challenging. Therefore, in such regard, lignin-based model compounds have been utilized for quantum chemical calculations, for instance, guaiacyl glycerol-b-guaiacyl ether, veratrylglycerol-b-guaiacyl ether, phenethyl phenyl ether, dilignol and dibenzodioxicin *etc.* [31–38]. Most of the studies have aimed to elucidate the dissolution behaviour with ionic liquids system. It has been reported that the dissolution of lignin can be favored when ions having the ability to make strong hydrogen bonds and non-covalent interaction between lignin model and the solvents are used. Zhang et al. [35], performed a detailed DFT study for lignin-based model, guaiacyl glycerol-β-guaiacyl ether model dissolution using ionic liquids formed by different cations and anions, and demonstrated that hydrogen-bond formation between lignin model and anion is crucial for dissolution. Anions are predominantly forming hydrogen bonds with α-OH; however, anions with higher number electronegative atoms or conjugated electrons are more pronounced for lignin dissolution. Similarly, a combined experiment with DFT and molecular dynamics study has shown that toluene sulfonic acid (p-TsOH) hydrotrope exhibited higher lignin removal over other solvents such as ionic liquids and deep eutectic solvents. The C-H$\cdots\pi$ and strong hydrogen bonds are the driving factors for higher dissolution [36]. These investigations have been used as a fundamental concept that provides design and selection of appropriate solvent for dissolution. Although various lignin models with different solvents have been demonstrated for quantum chemical investigation, lignin model with organic solvents changing the polarity is still uncommon.

The present study mainly focuses on the investigation of fractionation process with different organic solvents. The organic solvents were chosen based on polarity, for instance, ethanol and acetone (highly polar), diethyl ether (moderately polar) and hexane (non-polar). Hardwood kraft lignin was considered for the fractionation process with aforementioned solvents and followed by the investigation of soluble and insoluble fraction using gel permeation chromatography (GPC), pyrolysis gas chromatography mass spectrometry (Py-GC–MS) and near-infrared spectroscopy (NIR) measurements. Subsequently, DFT calculations were employed for the lignin model, dibenzodioxicin (DBD) with solvents, to illustrate the lignin fractionation mechanism and understand the driving force during fractionation process. Furthermore, to the best of our knowledge, this is the first study that combines experimental and theoretical analyses to elucidate the impact of only organic solvents in the fractionation process.

2. Materials and methods

2.1. Materials

For the experimental part, hardwood kraft lignin (HKL) was used. HKL was isolated by precipitation from industrial hardwood black liquor from *Eucalyptus* sp. using sulfuric acid (98%) as acidifying agent (pH = 2). The precipitated HKL was filtered and washed until neutral pH, dried at 25 °C and stored for further studies. The organic solvents used for the fractionation process were ethanol (absolute, Scharlab), acetone (Scharlab), diethyl ether (Fisher) and hexane (Fisher). Other solvents and reagents used for lignin characterization were *N*,*N*-Dimethylformamide (99.5%, Fisher Chemical, UK) and Lithium bromide (PanReacQuímica SAU, Spain).

2.2. Single-step fractionation of hardwood kraft lignin

Lignin fractions were extracted from the crude HKL using organic solvents of different nature (ethanol, acetone, diethyl ether and hexane) in a single-step fractionation process. HKL (1 g) was suspended in 50 mL of solvent with a constant stirring (1000 rpm) at room temperature for 2 h. The soluble (FS) and insoluble (FI) fractions were separated by filtration. FI was washed and dried in vacuum at 30 °C overnight, while FS was recovered by removing the solvent under reduced pressure in a rotary evaporator. The experiments were carried out in triplicate in order to check the replicability of the single-fractionation process. The yields of the fractions were calculated on dry basis. The Pearson correlation coefficient was calculated from the data set of yields, average molecular weight and polarity of solvents using OriginPro 2015 software.

2.3. Structure characterization

The molecular weight-average (Mw), number-average (Mn) and polydispersity (Mw/Mn) of kraft lignin (HKL) and isolated lignin fractions were determined by Gel permeation chromatography (GPC) (Jasco LCNet II/ADC), equipped with an RI-2031 Plus Intelligent refractive index detector, PolarGel-M column (300 mm 7.5 mm) and PolarGel-M guard (50 mm 7.5 mm). For the test, 0.25 mg of the sample were dissolved in 5 mL of N,N dimethylformamide (DMF) with 0.1% lithium bromide, and 20 μL of solution were injected. The column operated at 40 °C and eluted with N,N dimethylformamide (DMF) with 0.1% lithium bromide at flow of 0.7 mL/min. Monodispersed polystyrene was used as a calibration standard.

Pyrolysis gas chromatography mass spectrometry (Py-GC–MS), equipped with a 5150 Pyroprobe pyrolyzer (CDS Analytical Inc., Oxford, PA) and GC–MS instrument (Agilent Techs. Inc. 6890 GC/5973MSD), were used to study the monomeric composition of lignin. A quantity between 400 and 800 mg was pyrolyzed in a quartz boat at 600 °C for 15 s with a heating rate of 20 °C/ms (ramp-off) with the interface kept at 260 °C. The pyrolyzates were purged from the pyrolysis interface into the GC injector under inert conditions using helium gas. The fused-silica capillary column used was an Equity-1701(30 m × 0.20 mm × 0.25 μm). The GC oven program started at 50 °C and was held for 2 min. Then it was raised to 120 °C at 10 °C/min and was held for 5 min. After that, it was raised to 280 °C at 10 °C/min. and held for 8 min; it was finally raised to 300 °C at 10C/min and held for 10 min. The compounds were identified by comparing their mass spectra with the National Institute of Standards Library (NIST) and with compounds reported in the literature [39–41]. Only compounds with peak area ratio higher than 0.2% were selected for the calculation. The sum of these peak areas was normalized to

100% to determine the compounds relative abundance since the peak area is widely related to the concentration of each compound.

2.4. NIR spectroscopy and chemometric analyses

Near infrared spectral measurements were performed in a Bruker MPA II spectrophotometer equipped with an integrating sphere accessory. NIR spectrum of lignin sample was recorded on diffuse reflectance mode from an average of 64 scans over the range 12,000–4000 cm^{-1} at a spectral resolution of 8 cm^{-1}. HKL and its fractions were freeze-dried for 24 h to remove the moisture content and avoid any moisture interference during NIR spectra collection. Three measurements were performed on each sample. Then extended multiplicative scatter correction (EMSC), followed by an average, were applied to the three measured spectra on each sample in order to remove the scatter and have more representative processed spectra.

NIR spectra were analyzed using SoloMIA (Eigenvector Research, Inc., Wenatchee, WA, USA), preprocessing the NIR spectra by using extended multiplicative scatter correction (EMSC), SVN and mean center. Principal component analysis (PCA) and partial least squares (PLS) regression modeling were applied on preprocessed NIR spectra. Cross validation of calibration was conducted, principal components (PCs) or latent variants (LVs) were selected, and the associated root mean square error of cross validation (RMSECV) value obtained.

2.5. Density functional theory (DFT) calculations

Lignin is a complex aromatic biopolymer and a rather expensive one on which to perform quantum mechanical DFT calculations. Furthermore, the macro molecular structure of lignin is hardly known. In such case, a series of model compounds containing various linkages (such as β-O-4, α-O-4, β-β, β-1 and 5-5′) are focused for DFT calculations [35,36,42–44]. In this work, a typical model compound, dibenzodioxocin (DBD), is considered (shown in Fig. 1). The primary purpose of this selected model is to incorporate as much as possible the different linkages. The selected lignin model contains three predominant linkages, β-O-4, α-O-4 and 5-5′, and present about 10% in softwood lignins.

All DFT calculations were performed using GAMESS-US [45] package with wB97D-2 level of theory and 6-311g(d,p) basis set. This typical dispersion corrected functional shows a greater ability to describe the hydrogen bond and Van der Waals interaction between the molecules as they play crucial roles in many chemical systems. The basis set used in this study was 6-311g(d,p) without any diffusion function. The recent study revealed that extra-diffuse function does not influence the interaction energy, H-bonding and O—H stretching frequencies [46,47]. The isolated structure of DBD was optimized in gas phase and different solvent environments (ethanol, acetone, diethyl ether and hexane) using solvation model density (SMD) [48] method. In the following, single-point energy calculation was performed for different configurations with each solvent in order to find the most possible interaction. The lowest energy configuration of four to six configurations was selected for further optimization with wB97D-2/6-311g(d,p) level of theory to find the final geometry. Vibrational analysis was carried out for all final investigated geometries to ensure no imaginary frequencies were obtained, confirming each geometry has a minimum on the potential energy surface. Zero-point energy corrections were also included, and the energy of all systems was estimated at temperature $T = 298.15$ K.

After optimizations of all investigated geometries, Jmol [49] and WxMacMolPlt [50] were used for visualization. Atoms in molecules (AIM) theory has been used to account hydrogen-bond characteristics such as nature of hydrogen-bond and strength using electron density (ρ_{BCP}) and Laplacian of electron density ($\nabla^2\rho_{BCP}$) [51,52]. These parameters are calculated at the bond critical point (BCP) with the criteria of $\nabla^2\rho_{BCP} > 0$ for hydrogen bonds and ionic bonds and $\nabla^2\rho_{BCP} < 0$ for covalent bonds. Reduced density gradient (RDG) scatter plots and non-covalent interaction (NCI) plots are potentially used to illustrate non-covalent interaction between the molecules [53,54]. These analyses, along with atomic changes (ChelPG) [55], were extracted using Molden [56] and Multiwfn [57] packages.

The interaction energy (ΔE) of the different configurations has been expressed as the energy difference of the most stable configuration and corresponding isolated geometries,

$$\Delta E = 2625.5 \times (E_{ab} - E_a - E_b), kJ\ mol^{-1}$$

where E_{ab} represents lignin DBD model with solvent configuration, and E_a and E_b are the energies for isolated geometries of lignin DBD model and solvents (ethanol, acetone, diethyl ether and hexane), respectively.

3. Results and discussion

3.1. Yields and solubility of hardwood kraft lignin in organic solvents

In this work, industrial hardwood kraft lignin was treated with organic solvents of different chemical nature and polarity using a single-step fractionation process in order to evaluate the chemical characteristics of the resulted soluble and insoluble fractions.

The solvents were classified according to their chemical nature in addition to their polarity and hydrogen-bonding capacity based on the Hansen solubility parameters. Ethanol ($\delta_P = 8.8$; $\delta_H = 19.4$) was used as a polar protic solvent, while acetone ($\delta_P = 10.4$; $\delta_H = 7.0$) was selected as a polar aprotic solvent. Moreover, non-polar solvents diethyl ether ($\delta_P = 2.9$; $\delta_H = 5.1$) and hexane ($\delta_P = 0$; $\delta_H = 0$) were used for kraft lignin fractionation.

The yields of soluble and insoluble fractions from the single-extraction processes are presented in Fig. 2. According to previous work, the solubility of lignin compound in organic solvents relies on lignin type [19,26]. HKL has been produced from kraft cooking of *Eucalyptus* chips. During the pulping process, lignin is partially degraded by the cleavage of aryl ether bonds, allowing its dissolution in the black liquor [58]. This technical lignin is characterized by having a high content of phenolic hydroxyl groups and the presence of condensed chemical structures as a result of the kraft pulping process. This technical lignin is characterized by having a high content of phenolic hydroxyl groups and the presence of condensed chemical structures as a result of the kraft pulping process [9,59].

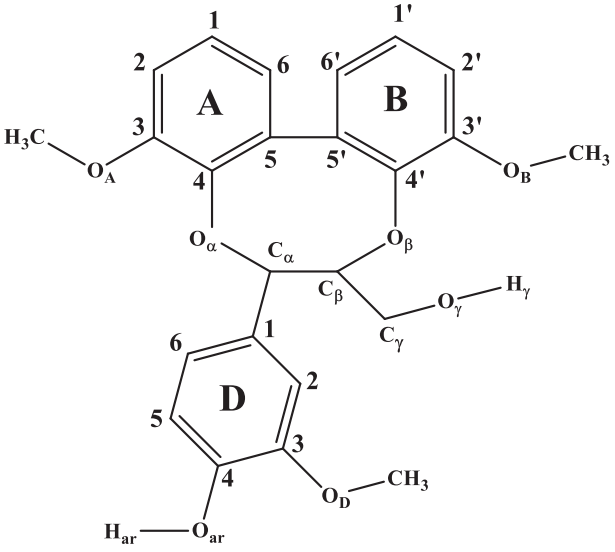

Fig. 1. Structure of a lignin model used in the current study.

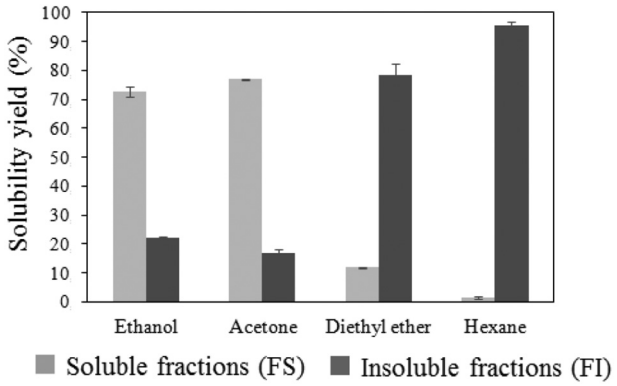

Fig. 2. Solubility yields of HKL in different organic solvents.

Results revealed a linear correlation between the polarity of the solvents and yields of soluble fractions ($R = 0.97$). Therefore, high solubility (70–80%) of HKL was observed in polar protic and aprotic solvents such as ethanol and acetone. Other authors also reported the ability of these organic solvents to solubilize high yield of starting lignin [22,60]. Diethyl ether was able to solubilize around 11% of HKL; however, extracted soluble fractions from hexane (<1%), which were analyzed by GC–MS technique, were solely based on lipophilic fraction (fatty acids) present in the kraft lignin. Previous research study on Eucalyptus kraft lignin fractionation using organic solvents of an increasing hydrogen-bonding capacity for a sequential extraction proved that hexane and diethyl ether also provided very low solubilization yield of lignin with values of 0.2% and 1.6%, respectively [61].

3.2. Structural characteristics of lignin fractions

For better understanding the effect of organic solvent of diverse nature on the hardwood kraft lignin structure, the molecular weight distributions of both soluble and insoluble fractions were examined. The average molecular weight and polydispersity results are shown in Table 1 and GPC chromatograms are presented in Fig. S1 of the supplementary information. Due to the chemical differences between lignin and calibration polystyrene standards, the results of molecular weight distribution of HKL and its fractions has been considered as relative values of molar mass.

In general, soluble fractions presented lower molecular weights and higher homogeneity than initial hardwood kraft lignin, while remaining insoluble fractions showed higher molecular weights and polydispersity, especially as derived from ethanol and acetone fractionation processes. Duval and co-workers showed high average molecular weight and polydispersity values for insoluble softwood kraft lignin fractions from solvents such as methanol, ethanol, propanol, acetone, methyl ethyl ketone and ethyl acetate [22]. This effect was also observed by Sadeghifar and Argyropoulos in pure acetone fractionation of softwood kraft lignin [60]. In that work, the molecular weight for the unfractionated lignin was determined to be about 6000 g/mol (PDI = 4.0) and 3500 g/mol (PDI = 3.5) for soluble acetone lignin fraction. However, the analysis of insoluble fraction showed significantly higher molecular weight (Mw = 14,000) and wider molecular weight distribution (PDI = 6.6). In addition, fractionation of lignin from different origins in acetone-water solutions containing above 50% acetone (v/v) also revealed that remaining insoluble fractions had higher molecular weight than parent lignin and a wide molecular mass distribution [28]. This phenomenon is related to lignin association in organic solvents where the π-π interaction of the aromatic rings was proposed to be the mechanism of lignin aggregation [62]. This effect was especially appreciable in insoluble kraft and alkali lignins, but not in organosolv lignins [63].

In this work, a clear correlation was found between molecular weight of soluble and insoluble lignin fractions with the polarity of the solvents ($R = 0.99$ and $R = 0.95$, respectively). Moreover, the polydispersity index of soluble fractions was highly correlated with the polarity of the solvent ($R = 0.98$). Therefore, these results suggest that the polarity of organic solvents plays an important role to control the molecular properties of lignin during a fractionation process. Solvents with lower polarity, but not totally non-polar like hexane, are able to extract more homogenous lignin fractions with lower molecular weights. It was remarkable the low molecular weight and low heterogeneity of soluble lignin fraction extracted with diethyl ether. As was reported in a previous study where the solubility of Alcell® lignin in various solvents was investigated, lignin was slightly soluble in diethyl ether but allowed the isolation of very homogeneous low molecular weight fraction [27]. Insoluble fractions from ethanol and acetone resulted in high molecular weight heterogeneous lignin fractions, which was consistent with previous research [22,60].

Furthermore, analytical pyrolysis (Py-GC–MS) of lignin samples was carried out to study the characteristics of the resealed lignin-derived compounds distribution and assess the effect of organic solvents in the lignin composition. The pyrograms from hardwood KL as well as soluble and insoluble fractions are presented on the Fig. S2 of the Supplementary Information. Pyrolytic products from lignin usually involve phenolic compounds, furans and long-chain carboxylic acids and esters [64]. Phenolic compounds are associated with the monomeric composition and chemical structure of lignin polymer while furan derivatives originate from the degradation of polysaccharides and their fragmentation [65], and the presence of fatty acids is commonly associated with the origin and their resistance to thermo-chemical extraction processes [66].

Fig. 3 represents the relative content of identified products according to their origin. As can be observed, phenolic area detected for soluble fractions was similar to that found for HKL, while the total phenolic area found for insoluble fractions was substantially lower, especially in the case of ethanol and acetone. This result can be related to their high molecular weight. Moreover, a clear relation was found between the

Table 1
Molecular weight-average (Mw), number-average (Mn) and polydispersity (PDI) of HKL and isolated lignin fractions determined by GPC.

	Soluble fractions			Insoluble fractions		
	Mn (g/mol)	Mw (g/mol)	PDI (Mw/Mn)	Mn (g/mol)	Mw (g/mol)	PDI (Mw/Mn)
Hardwood KL	669	2477	3.7	–	–	–
Ethanol	633	1982	3.1	1762	8492	4.8
Acetone	661	2251	3.4	1670	10,384	6.2
Diethyl ether	412	563	1.4	759	2894	3.8
Hexane	–	–	–	676	2569	3.8

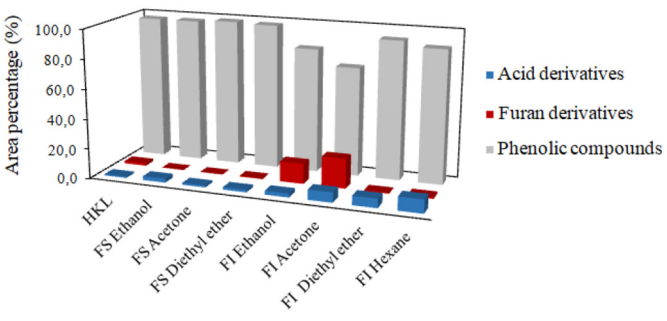

Fig. 3. Relative content of identified pyrolysis products according to their origin.

Table 2
Relative content (%) of phenolic-type compounds and their classification according to their structural characteristics.

	HKL	Ethanol		Acetone		Diethyl ether		Hexane	
		FS	FI	FS	FI	FS	FI	FS	FI
Phenolic compounds: origin									
H-type	1.4	1.1	3.9	2.1	3.0	1.5	2.7	–	2.0
G-type	16.5	21.8	21.5	24.1	17.1	15.4	17.2	–	18.6
S-type	62.7	60.5	45.8	58.3	42.7	60.0	60.9	–	57.1
Ca-type	16.7	14.0	12.5	14.2	10.4	20.9	12.4	–	12.0
S/G	4.8	3.4	2.7	3.0	3.1	5.2	4.3	–	3.7
Phenolic compounds: structure of the side chain									
Non-substituted saturated chains (%)	29.9	30.8	25.6	34.5	16.5	40.1	21.7	–	25.0
Oxygenated groups in the side chains (C=O) (%)	1.4	6.5	2.3	2.0	5.1	3.6	18.6	–	9.6
Unsaturated side chains (C=C) (%)	6.7	5.7	10.9	6.6	9.0	3.5	7.4	–	6.6
Short chain (C1 + C2)	36.1	40.0	35.5	40.7	27.2	45.7	42.8	–	37.2
Long chain (C3)	2.1	3.3	5.5	3.4	3.7	2.3	4.7	–	4.9
(ArC1 + ArC2)/ArC3	17.1	12.0	6.5	11.8	7.4	20.2	9.0	–	7.5

yield of soluble fraction and amount of phenolics released during the fast pyrolysis of the insoluble fraction from the same process. These results indicated that the solvents with high polarity like acetone and ethanol have a negative effect on quality of the remaining insoluble fractions. In addition, it was noticed a high number of furan-related compounds in insoluble fractions of ethanol and acetone. It is well known that lignin and carbohydrate moieties are chemically bound in native biomass, forming a lignin-carbohydrate complex (LCC). These strong chemical bonds between lignin and hemicellulose greatly affect the purity of lignin and hemicellulose during their isolation [67]. It was previously reported the alkaline stability of LCC bonds during the kraft pulping process and presence of lignin-carbohydrate complex in the black liquor [68]. Therefore, the results suggest that kraft lignin chemically bonded to carbohydrates were not solubilized, remaining in the insoluble fractions. Previous studies showed similar results [22,63,69]. The high molecular weight of insoluble fractions from ethanol and acetone was related to the carbohydrate-lignin complex structure, which contributes to their molecular weight characteristics.

In addition, released phenolic compounds were grouped into four categories according to their aromatic structure: phenol-type compounds (H), guaiacyl-type compounds (G), syringol-type compounds (S) and catechol-type compounds (Ca). Catechol-type compounds originated from the syringol-type compounds during a pyrolysis

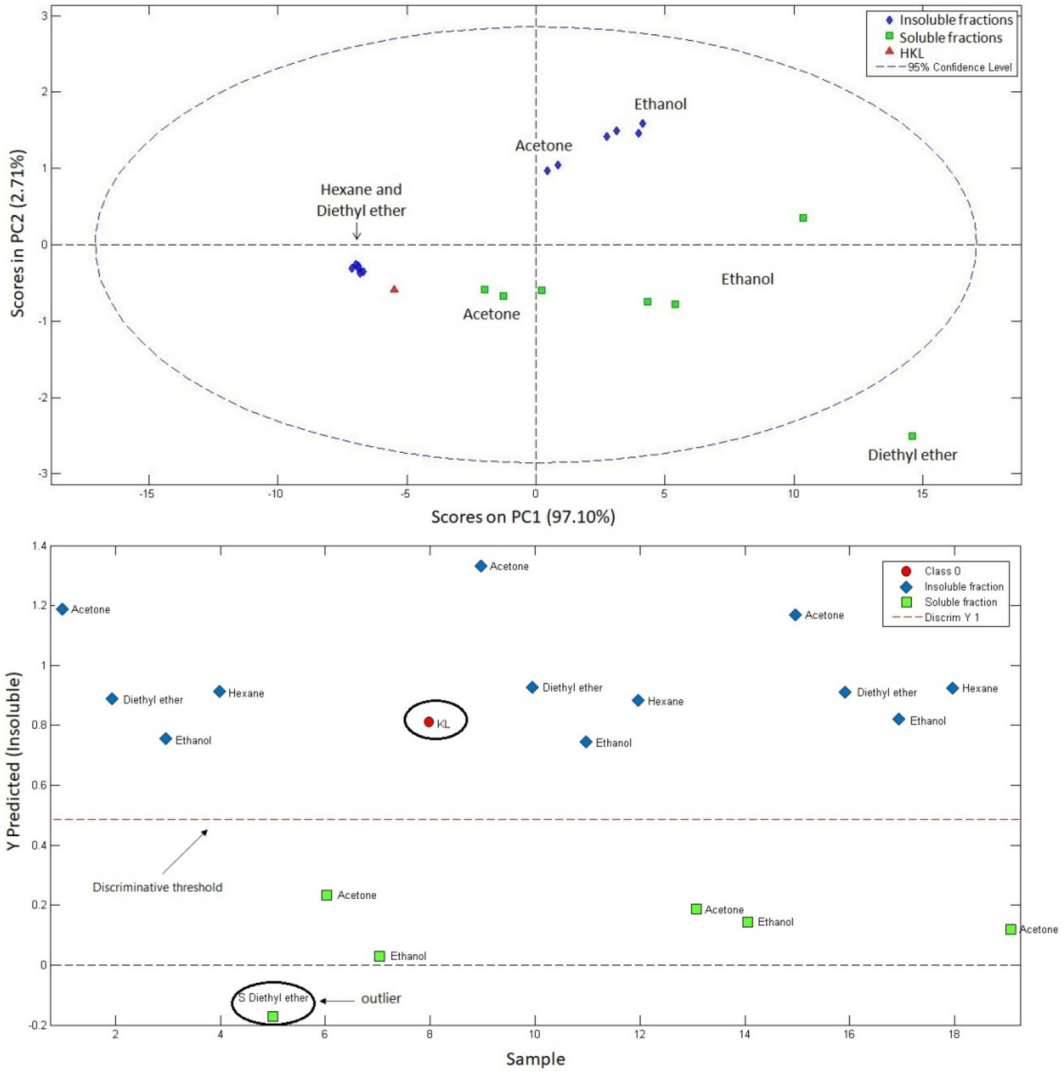

Fig. 4. Scores plot in the plane of PC1 *vs* PC2 and prediction plot for insoluble-soluble fractions.

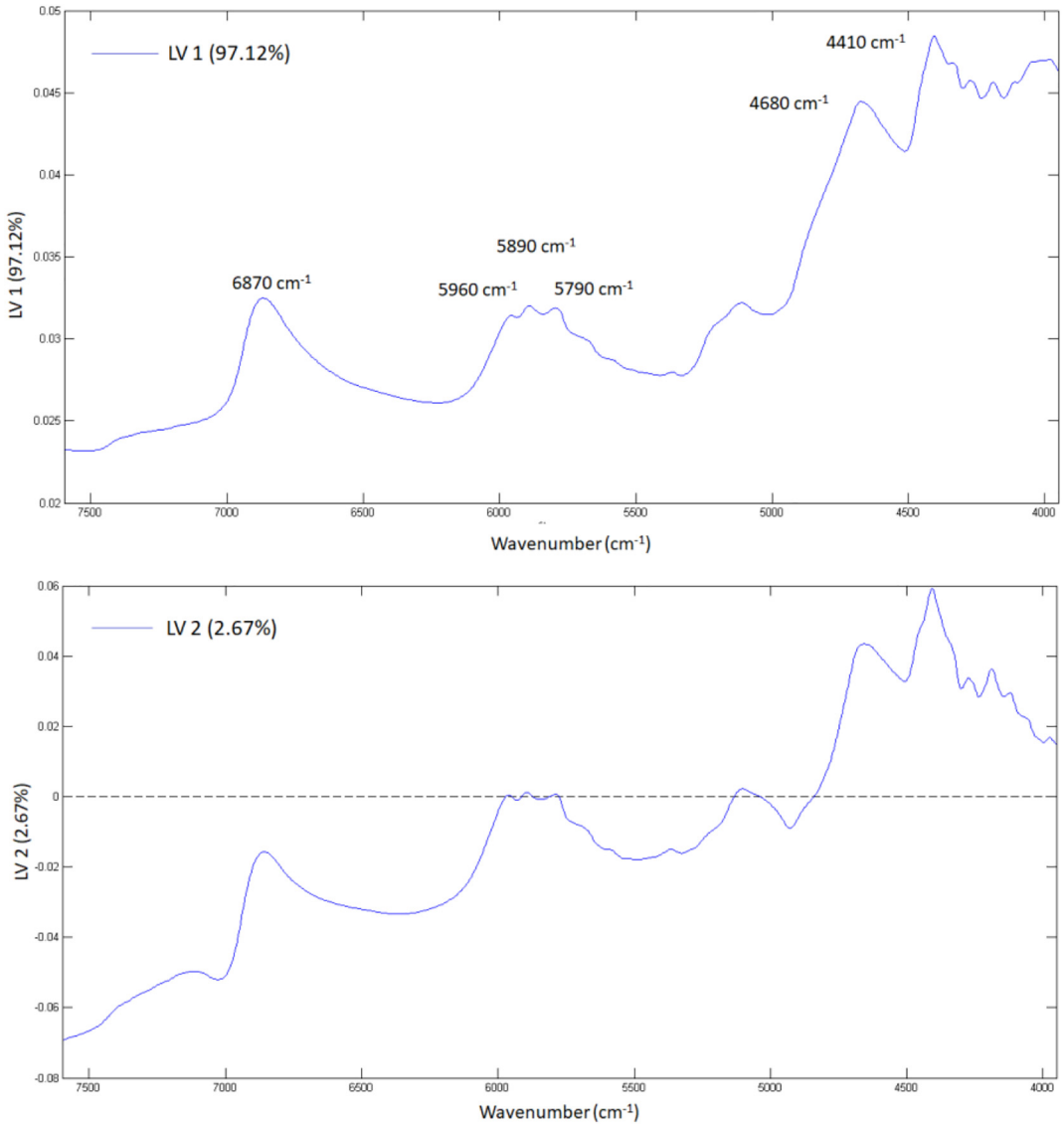

Fig. 5. Loadings of LV1 and LV2.

process as has been demonstrated by previous research studies [70,71]. Therefore, the syringyl/guaiacyl ratio (S/G) was calculated by dividing the sum of peak areas from syringyl units (including catechol derivatives) by the sum from the peak areas of guaiacyl derivatives. The presented results (Table 2) are from the average of three replicates. The main products of HKL and fractions were derived from S unit because they came from hardwood.

As can be observed in Table 2, an increase of G-type compounds was detected by analytical pyrolysis of both soluble and insoluble fractions, except for the soluble fraction coming from diethyl ether. A linear correlation was found between the polarity of the solvent and the increment of guaiacyl-derived compounds ($R = 0.99$). Park and co-workers have suggested that S-type units are less soluble in solvents; therefore, the resulted lignin fraction presented higher guaiacyl content in their chemical structure [19]. But this phenomenon is also observed in the case of insoluble lignins. Therefore, it could indicate that during solubilization on lignin in solvents demethoxylation reactions occur in the lignin, especially in polar solvents such as acetone and ethanol. Other authors also observed a reduction of methoxyl group content after lignin solubilization in organic solvents [27].

Furthermore, lignin-derived phenolic compounds were also classified according to their structure and characteristics of their side chain, and several differences were observed. Regarding compounds with non-substituted saturated chains, soluble fractions released higher content of lignin-derived products with this specific characteristic than starting HKL, while the opposite was observed for insoluble fractions. This indicates that soluble fractions contain more aliphatic saturated structures than initial HKL. It is remarkable the high content of released pyrolysis product with this particular chemical characteristic of FS from diethyl ether. The resulting structural characteristics using diethyl ether as a solvent for lignin polymer fractionation were also detected by Thring et al. [27]

No clear trend was observed for compounds with oxygenated groups in the side chains; however, it can be said that these compounds were more abundant in insoluble fractions, especially those that came from non-polar solvents. Moreover, the compounds with unsaturated side chain are not very representative of the original structure of lignin since C=C bonds can be formed during the pyrolysis process [72,73].

In addition, it was observed that the fractionation process using organic solvents, in general, generates lignins with higher content of aromatic structures with short aliphatic chain, except in the case of insoluble fractions of polar solvents. The effect of the solvent in the aliphatic chain of the resulted pyrolysis products can be clearly noticed by the short/long aliphatic chain ratio presented in Table 2.

Table 3
Selected structural parameters for optimized geometry of lignin model in gas phase and in presence of different solvents (ethanol, acetone, diethyl ether and hexane) at wB97X-D/6-311g(d,p) level of theory. A, B and D represent different phenyl rings present in the DBD structure. (See Fig. 3 for atom labels.)

Atoms	Gas	Ethanol	Acetone	Diethyl ether	Hexane
Bonds (Å)					
$C_\alpha - C_\beta$	1.525	1.525	1.525	1.525	1.525
$C_\alpha - O_\alpha$	1.442	1.450	1.448	1.446	1.444
$C_\alpha - D_{C1}$	1.509	1.508	1.508	1.509	1.509
$C_\beta - O_\beta$	1.416	1.419	1.419	1.418	1.417
$C_\beta - C_\gamma$	1.527	1.524	1.527	1.527	1.527
O_α – A4	1.365	1.371	1.368	1.366	1.365
O_β – B4′	1.353	1.358	1.354	1.354	1.353
$C_\gamma - O_\gamma$	1.404	1.414	1.409	1.407	1.405
$A_{C5} - B_{C5'}$	1.497	1.498	1.499	1.499	1.499
D_{C3}-O_D	1.365	1.371	1.367	1.366	1.365
O_D- C(H_3)	1.419	1.427	1.424	1.423	1.421
$B_{C3'}$-O_B	1.358	1.357	1.356	1.356	1.357
O_B-C(H_3)	1.410	1.419	1.418	1.416	1.413
A_{C3}-O_A	1.350	1.350	1.347	1.348	1.349
O_A-C(H3)	1.409	1.417	1.415	1.413	1.411
Angle (°)					
$C_\alpha - C_\beta - O_\beta$	107.7	107.6	107.4	107.5	107.5
$C_\alpha - O_\alpha - A_{C4}$	113.9	114.0	114.2	114.1	114.2
$D_{C1} - C_\alpha - C_\beta$	113.9	114.2	114.3	114.2	114.2
$D_{C1} - C_\alpha$ - O_α	113.5	113.5	113.6	113.6	113.5
$C_\alpha - C_\beta - C_\gamma$	113.2	113.0	113.4	113.3	113.3
$C_\beta - C_\gamma - O_\gamma$	110.5	110.4	110.3	110.4	110.5
$C_\beta - O_\beta - B_{C4'}$	123.2	123.0	123.2	123.3	123.4
$O_\alpha - C_\alpha - C_\beta$	110.1	109.5	109.6	109.7	109.8
$O_\beta - B_{C4'} - B_{C5'}$	127.6	128.0	127.9	128.0	128.1
$O_\alpha - A_{C4} - A_{C5}$	120.9	120.8	120.9	120.9	121.0
DC_3-O_D-C(H3)	114.5	113.8	114.1	114.2	114.4
$B_{C3'}$-O_B-C(H3)	117.7	117.8	117.8	117.8	117.9
A_{C3}-O_A-C(H3)	118.0	118.0	118.2	118.1	118.1
$O_\alpha - C_\alpha - C_\beta$ - O_β	53.6	53.5	53.9	54.0	53.9
Charges (e)					
C_α	0.4882	0.5465	0.6048	0.5631	0.5041
C_β	−0.1261	−0.2128	−0.2153	−0.1819	−0.1741
C_γ	0.4286	0.4482	0.4173	0.4376	0.4464
O_α	−0.4725	−0.5312	−0.5272	−0.5101	−0.4778
O_β	−0.3291	−0.3411	−0.3552	−0.3311	−0.3201
O_γ	−0.6066	−0.6682	−0.6290	−0.6264	−0.6213
O_D	−0.4096	−0.4459	−0.4401	−0.4301	−0.4184
$C(H_3)_{OD}$	0.2121	0.2073	0.2532	0.2441	0.2266
O_A	−0.2709	−0.3053	−0.2823	−0.2765	−0.2737
$C(H_3)_{OA}$	0.1328	0.1142	0.1157	0.1135	0.1140
O_B	−0.2798	−0.3284	−0.3187	−0.3063	−0.2983
$C(H_3)_{OB}$	0.0298	0.0380	0.0443	0.0363	0.0327

3.3. Chemometrics analysis

As a complementary analysis, chemical information provided by NIR spectroscopy was processed and subjected to an exploratory data analysis by applying principal components analysis (PCA) and partial least squares discriminant analysis (PLS-DA).

PCA was used as an exploratory method, reducing the original variables into new sets of principal components (PCs), scores and loadings, while PLS-DA was used as a classification method, creating groups (latent variables LVs) that are able to be regressed on each other and on observed covariates thus discriminating groups.

The spectral variance in the range of 7500–4200 cm^{-1} was reduced with PCA into three principal components that include 99.96% of the variance. As can be observed in the scores plot (Fig. 4), soluble and insoluble fractions were clearly differentiated by plotting PC1 *vs* PC2, accounting for 99.81% of the existing variances in collected spectra.

The spectral groups corresponding to HKL and insoluble fractions from hexane and diethyl ether presented negative scores in PC1 and PC2, evidencing chemical similarities between them. However, insoluble fractions from ethanol and acetone showed positive scores in PC1 and PC2. Soluble fraction from diethyl ether appears as an outlier, indicating a total chemical difference with initial kraft lignin and other isolated fractions. The chemical analyses also proved similarities and differences between separated groups.

The PSL-DA divided the data set into three LVs (99.91%), predicting the insoluble-soluble fractions (probability 100%) with a distance between 0.6 (soluble acetone *vs* insoluble ethanol) and 1.5 (insoluble acetone *vs* soluble diethyl ether). HKL was predicted as insoluble in the range of the main insoluble fractions, except acetone, which was further away from the discriminative threshold. Moreover, the soluble diethyl ether fractions show negative values from the threshold, classifying it as an outlier.

Loadings (Fig. 5) evidence that the importance of the original variables (bands) mostly contributed to the separation of lignin samples in each PC and LV. The loading plot of LV1 showed similar shape than the mean spectra, which was expected from the mathematical treatment applied. In LV1, it is worth mentioning a positive influence of the bands at 6870, 5960, 5890, 5790, 4680 and 4410 cm^{-1}. These bands are totally related to chemical structure of lignin such as phenolic O—H groups, aromatic substructures and C—H stretching of -CH_2 groups and C=C and C—O stretching. Additionally, LV2 showed a positive intensity in the bands related to specific functional groups of lignin at 4680 and 4410 cm^{-1} [74].

3.4. DFT analysis of lignin model and solvent interactions

The isolated geometry of lignin DBD model in gas and different solvents were optimized, and selected bond parameters and charges are listed in Table 3. It is observed from Table 3 that polarity of the solvents significantly impacts the bond lengths, especially for $C_\alpha - O_\alpha$ bond. In such case, high polarity nature of ethanol elongates this bond around 0.008 Å, followed by acetone. The polarity of solvent decreases, and the bond length approaches to initial or gas phase value. For instance, in the case of hexane, $C_\alpha - O_\alpha$ bond deviates only 0.002 Å. A similar trend has been pronounced for $C_\gamma - O_\gamma$ bond, where ethanol shows a large influence. However, considering the $C_\beta - O_\beta$ bond, the changes are less pronounced in different solvent environments. Therefore, it is indicated that α- and γ-based atoms are the crucial sites for high polarity of solvents, for instance, ethanol and acetone. The bond lengths of methoxy side chain present in the aromatic moieties were also compared with different solvents. It was shown that the methoxy group in **D** ring, particularly, D_{C3}-O_D, exhibits a larger deviation than A_{C3}-O_A and $B_{C3'}$-O_B bonds for ethanol from gas phase. The extended π bond configuration between A and B rings can influence this small deviation of bond lengths. In contrast, a significant effect was observed for the bond between methoxy O and methoxy C, and the difference in bond length is about 0.009 Å for gas and ethanol solvent. However, the variation becomes small when decreasing the polarity of solvents. Furthermore, it is noted that 5-5′ ($A_{C5} - B_{C5'}$) linkage in the lignin model does not undergo any changes at different solvent environments due to the fact of partial double bond character and π electrons delocalization. The investigated solvents do not significantly modify the calculated bond angles and dihedral angles, except for $O_\alpha - C_\alpha - C_\beta$ and DC_3-O_D-C(H3) angles. In addition to the selected structural characteristics, the atomic charge distributions were also calculated by ChelpG method to

Table 4
Interaction energy (ΔE) values for lignin model with different solvents in kj/mol.

Lignin DBD model – solvent	ΔE (kj/mol)
Lignin – EtOH	−55.53
Lignin – ACE	−48.08
Lignin – DEE	−46.74
Lignin – HEX	−45.01

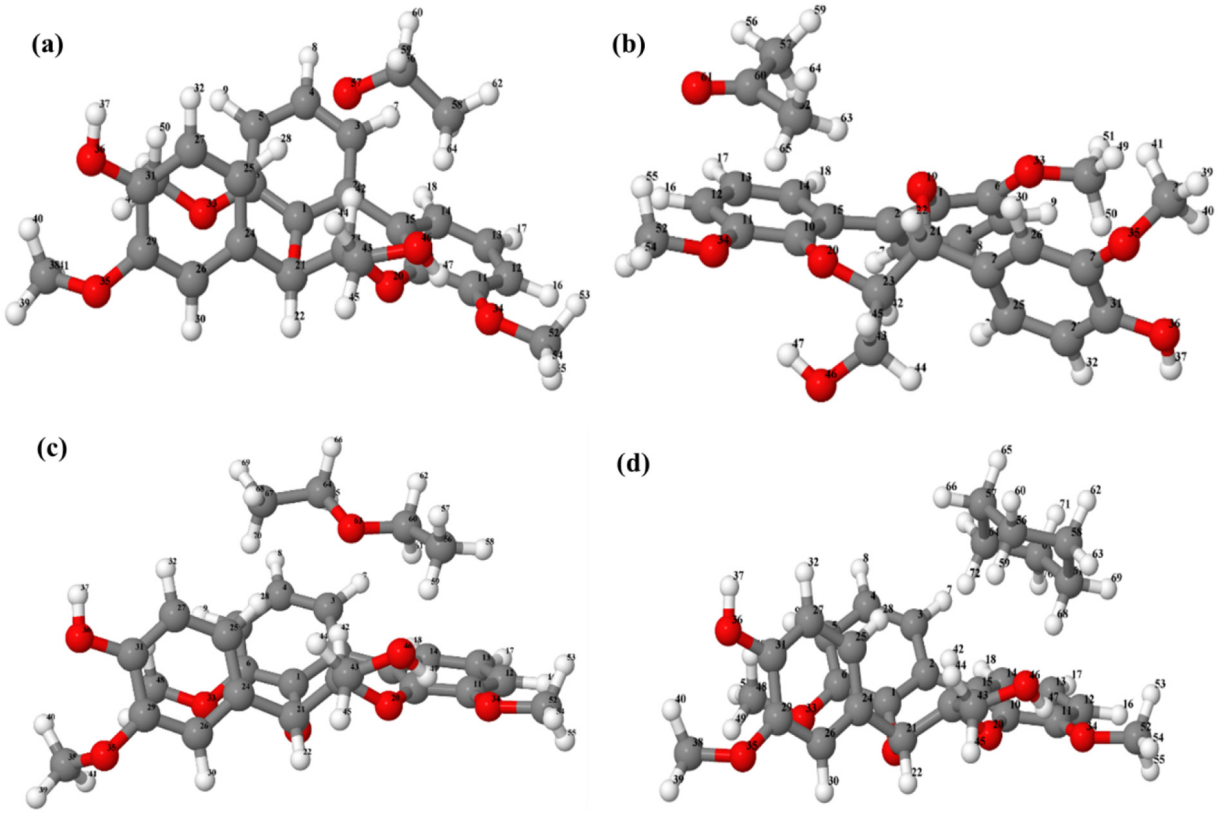

Fig. 6. Optimized geometry of (a) lignin DBD – ethanol, (b) lignin DBD – acetone, (c) lignin DBD – diethyl ether and (d) lignin DBD – hexane.

investigate the influence of solvents. From Table 3, it is also observed that the charges associated with ethanol and acetone exhibit a significant difference from gas phase isolated geometry than low polar solvents (diethyl ether and hexane). An important deviation, around 0.06 e, can be seen for O_α, O_γ than O_β, which demonstrated that β site is less evident.

3.5. Optimization of lignin DBD model with solvents

The lignin DBD model was optimized with solvents to illustrate the most possible interaction, and interaction energies are presented in Table 4. It is observed from Table 4 that lignin model with ethanol exhibits the highest interaction energy values among other lignin – solvents. The second highest interaction energy was obtained for lignin model with acetone, and the difference in energy between ethanol and acetone was about 7.5 kj mol^{-1}. It should be noted that the least interaction was obtained for lignin model with non-polar hexane; however, the difference in energy associated with diethyl ether was small at 1.73 kj mol^{-1}. This finding is in full agreement with the experimental part that lignin fraction using ethanol solvent owns high yield compared to the least yield observed form hexane.

We have also optimized the lignin model with different solvents to demonstrate the most possible interaction, and optimized geometry structures are shown in Fig. 6, together with some optimized bond parameters. It can be seen from Fig. 6 that solvents such as ethanol, diethyl ether and hexane tend to approach the β-O and γ-OH, except for the case of lignin model with acetone, in which acetone bound to methoxy group and α-O bond. From the obtained bond parameters (Table 5), it is obvious that a significant change in bond length was observed for C_α-O_α, C_β-O_β and C_γ-O_γ bonds with ethanol solvent; whereas, the impact of hexane solvent is minimum. The bond length C_β-C_γ is elongated around 0.06 Å in the presence of diethyl ether than other solvents. However, no conformational change can be seen for the diethyl ether solvent after optimization. Similarly, comparing bond angles, the predominant effect was observed in lignin model for diethyl ether interaction than other solvents where the minimum deviations are noticed. The particular results can be seen for $C_\alpha - O_\alpha - A_{C4}$, $C_\alpha - C_\beta - C_\gamma$, $C_\beta - C_\gamma - O_\gamma$ and $C_\beta - O_\beta - B_{C4'}$. The linear conformation of diethyl ether could influence this particular change in the structural properties, despite its low polarity. The ChelpG charge distribution of lignin-solvent configuration shows that investigated solvents impact the lignin DBD model compared to DBD model without solvent, which is again more evident for the stronger interaction during fractionation process (Table 5).

3.6. Hydrogen bond analysis of lignin DBD model with solvents

We have performed AIM analysis proposed by Bader [51] to illustrate and classify the nature of intermolecular interaction between molecular systems. The intermolecular interaction parameters of ρ_{BCP} (charge density), $\nabla^2\rho_{BCP}$ (Laplacian of the charge density) and total energy density (H) are presented in Table 6. The corresponding AIM molecular bond critical point (BCP) graphs for lignin DBD model with different solvents, representing important hydrogen bonds, are illustrated in Fig. 7. In general, the typical criteria for ρ_{BCP} and $\nabla^2\rho_{BCP}$ to account hydrogen-bonds at BCP should be in the range of 0.002–0.035 a.u. for electron density and 0.024–0.139 a.u. for its Laplacian value [35,75]. The obtained hydrogen bonds for the investigated atom pairs in the proposed range explain that the solvents make hydrogen bonds with lignin DBD model. As can been from Fig. 7, solvents make stronger hydrogen bonds with lignin model, however; it is evident that the corresponding hydrogen-bonds rather weak compared to strong hydrogen bonds. This is due to the fact that there are fewer hydrogen donor/acceptor atoms present in the lignin model. It can be clearly seen from

Table 5
Selected structural parameters for entire optimized geometry of lignin model with different solvents (ethanol, acetone, diethyl ether and hexane) in gas phase. A, B and D represent different phenyl rings present in the DBD structure. (See Fig. 3 for atom labels.)

Atoms	DBD alone	DBD-Ethanol	DBD-Acetone	DBD-Diethyl ether	DBD-Hexane
Bonds (Å)					
$C_\alpha - C_\beta$	1.525	1.522	1.525	1.525	1.526
$C_\alpha - O_\alpha$	1.442	1.447	1.445	1.440	1.439
$C_\alpha - D_{C1}$	1.509	1.509	1.509	1.508	1.511
$C_\beta - O_\beta$	1.416	1.420	1.415	1.417	1.414
$C_\beta - C_\gamma$	1.527	1.528	1.528	1.533	1.530
O_α – A4	1.365	1.363	1.368	1.364	1.365
O_β – B4′	1.353	1.350	1.354	1.352	1.354
$C_\gamma - O_\gamma$	1.404	1.408	1.403	1.404	1.405
$A_{C5} - B_{C5'}$	1.497	1.496	1.496	1.499	1.498
Angle (°)					
$C_\alpha - C_\beta - O_\beta$	107.7	109.5	108.0	106.9	108.0
$C_\alpha - O_\alpha - A_{C4}$	113.9	114.7	113.5	115.3	114.4
$D_{C1} - C_\alpha - C_\beta$	113.9	114.3	113.9	113.5	112.7
$D_{C1} - C_\alpha - O_\alpha$	113.5	113.5	113.1	114.0	114.5
$C_\alpha - C_\beta - C_\gamma$	113.2	113.9	112.8	112.0	112.4
$C_\beta - C_\gamma - O_\gamma$	110.5	110.6	110.6	111.4	111.2
$C_\beta - O_\beta - B_{C4'}$	123.2	123.2	123.7	122.6	122.6
$O_\alpha - C_\alpha - C_\beta$	110.1	109.5	110.2	110.0	110.1
$O_\beta - B_{C4'} - B_{C5'}$	127.6	128.0	128.2	127.8	127.8
$O_\alpha - A_{C4} - A_{C5}$	120.9	121.3	120.8	121.6	121.6
$O_\alpha - C_\alpha - C_\beta - O_\beta$	53.6	54.8	54.2	51.1	48.4
Charges (e)					
C_α	0.4882	0.4953	0.4112	0.6166	0.4058
C_β	−0.1261	−0.2675	−0.1798	−0.1950	−0.3077
C_γ	0.4286	0.3636	0.4182	0.3889	0.3161
O_α	−0.4725	−0.4747	−0.4337	−0.5101	−0.4637
O_β	−0.3291	−0.3170	−0.2550	−0.3420	−0.2495
O_γ	−0.6066	−0.5897	−0.5882	−0.5924	−0.5341

the Fig. 7 that the electronegative oxygen present in the ethanol, acetone and diethyl ether bond with hydrogen atoms attached to alkyl carbon or aromatic carbon. The same phenomenon was observed from lignin DBD model to solvents, in which oxygen atoms from DBD model interact with hydrogen atoms present in solvents. Comparing hydrogen bond length and electron density values indicate that ethanol strongly interacts with lignin DBD model through strong hydrogen bond. The particular hydrogen-bond is formed between electronegative oxygen from ethanol and H atom from aromatic ring (O57⋯ H28) and the distance is about 2.222 Å, which is lower than that of other solvents, and the second strongest hydrogen-bond is observed for ethanol O and H from C_β. After ethanol, acetone forms strong hydrogen bonds through carbonyl oxygen with hydrogen from methoxy carbon, and the corresponding electron density (0.0117 a.u) is almost the same as diethyl ether (0.0116 a.u), despite lower hydrogen bond distance. The least hydrogen bonds were observed for hexane solvent. It is interesting to note that oxygen at γ-position significantly participates hydrogen bonding with all solvents except acetone. The hydrogen bond from γ-position is prevalent for diethyl ether and hexane solvents. A similar trend was also observed in previous works [35,36] where authors reported the hydroxyl groups at α- and γ-positions significantly participate the hydrogen bonding with solvents investigated. The positive values of Laplacian for electron density at BCP show that these investigated hydrogen-bonds are non-covalent. Similarly, positive values of energy density (H_{BCP}) in Table 6 reveal that these hydrogen-bonds have electrostatic properties. From the analysis, the observed hydrogen bond strengths follow the order of ethanol > acetone > diethyl ether > hexane. These particular results again revealed that ethanol is the most effective and pronounced solvent for fractionation process, which is consistent with experimental findings.

3.7. Reduced density gradient (RDG) analysis of lignin DBD model with solvents

Reduced density gradient (RDG) is another useful method to account non-covalent interaction, like AIM method, and provide reliable data. In this method, RDG is plotted against electron density multiplied by the sign of second eigenvalue (sign(λ_2)ρ) [54] and both inter- and intra-molecular weak interactions can be seen from Fig. 8. RDG scatter points indicate H-bonding interactions at negative scale (blue color), and the spikes (green color) and positive scale of sign(λ_2)ρ represent Van der Waals interactions and steric repulsions, respectively. Non-covalent interaction (NCI) analysis is used to visualize the respective interactions with graphical visualization in a real space. As stated in the hydrogen bond AIM analysis, the investigated system exhibits slightly weaker hydrogen bond, hence, a small negative value is evident. Fig. 8 (a–d) shows the RGD points (left) together with NCI plot (right), in which the strong intermolecular interaction of each case was circled. Ethanol demonstrates the strongest hydrogen-bond (−0.0145 a.u.) among the cases, and the lowest H-bond was obtained for hexane solvent (−0.0085 a.u.). The RDG points (marked with black circles) correspond to O57 ⋯ H28, O61 ⋯ H55, H59 ⋯ O46 and O46 ⋯ H28 for lignin model with ethanol, acetone, diethyl ether and hexane, respectively. Furthermore, NCI plots shown in Fig. 8 illustrate with the circled disk-shaped blocks that indicate non-covalent interactions between lignin model and solvents, and the hydrogen-bonds. Due to the fact of

Table 6
Hydrogen bond length (Å) and corresponding characteristics, ρ_{BCP} (charge density in a.u), $\nabla^2\rho_{BCP}$ (Laplacian of the charge density in a.u) and energy density (H in a.u) of lignin DBD model with different investigated solvents. (See Fig. 4 for atom labels.)

Lignin model – solvent	H-bonds	Length (Å)	ρ_{BCP} (a.u.)	$\nabla^2\rho_{BCP}$ (a.u)	H_{BCP} (10^{-2} a.u)
Ethanol	O57⋯ H28	2.222	0.0145	0.0501	0.1762
	O57 ⋯ H42	2.364	0.0127	0.0370	0.0847
	H64 ⋯ O46	2.502	0.0096	0.0264	0.0597
Acetone	O61⋯ H55	2.391	0.0117	0.0357	0.1227
	H63 ⋯ O19	2.475	0.0091	0.0283	0.0824
	H65 ⋯ O34	2.760	0.0059	0.0202	0.0682
Diethyl ether	H59 ⋯ O46	2.407	0.0116	0.0346	0.0886
	O63⋯ H42	2.591	0.0075	0.0222	0.0623
Hexane	O46 ⋯ H68	2.583	0.0085	0.0266	0.0791
	O46⋯ H59	2.584	0.0084	0.0255	0.0664

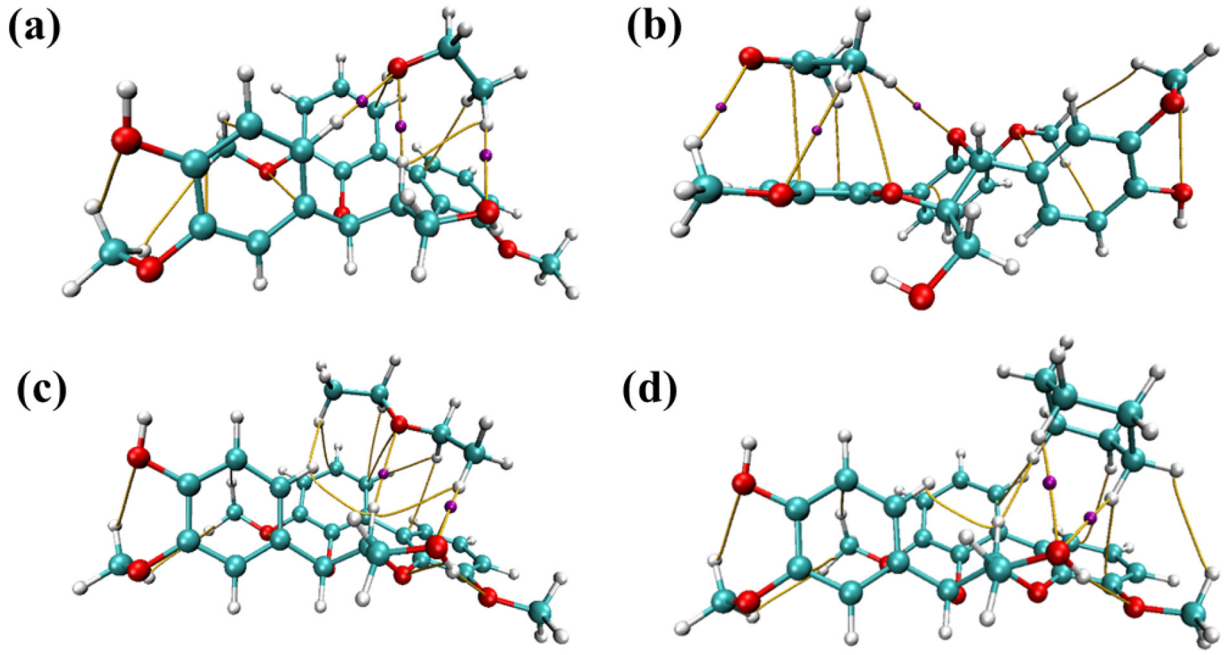

Fig. 7. Selected bond critical points (BCP) representing H-bonds between (a) lignin – ethanol, (b) lignin –acetone, (c) lignin – diethyl ether and (d) lignin – hexane. Color online: cyan – carbon, white – hydrogen, red – oxygen and pink – bond critical point of hydrogen bonds.

weak hydrogen bonds exist in the system, the non-covalent interactions displayed (red-circled) green color that represent weak inter-molecular interactions.

3.8. HOMO-LUMO band gap

HOMO-LUMO gap explains the stability and chemical reactivity of the molecule [76]. Large HOMO-LUMO represents the high kinetic stability and low chemical reactivity and, therefore, the trend is *vice-versa* for small HOMO-LUMO gap. Considering the investigated lignin-solvent systems (Fig. 9), lignin-ethanol system exhibits low band gap, which clearly illustrates higher chemical reactivity as compared to other systems. The second chemical reactivity has been obtained for lignin-acetone case. However, it should be noted that the difference in band gap energy associated with lignin-diethyl ether system to lignin-acetone is small. The least chemical reactivity or higher stability was obtained in the case of lignin-hexane system. These results again proposed that ethanol solvent interacts with lignin strongly and is susceptible to solubilize the lignin in a large quantity as compared to other solvent systems.

Overall, the obtained DFT results have demonstrated that the hydrogen bonds play a crucial role towards fractionation of lignin model compound. These results can be compared with several studies that used various solvents including ethylene glycol, choline chloride based deep eutectic solvents, recyclable acid hydrotropes (p-TsOH) and ionic liquids with different types of lignin models [35,36,77–80]. The results showed that hydrogen bond networks, charge transfer interactions and π-π staking are the predominant interactions that drive the fractionation process of lignin.

Conclusions based on the DFT calculation were consistent with the experimental results, where both methods found that ethanol makes stronger interaction with lignin, which eventually facilitates greater solubility. Indeed, experimental results have shown that ethanol and acetone drive demethoxylation reaction, which can be compared to the DFT-optimized isolated lignin model with different solvent environments where we have found some significant changes in the structural bond parameters with ethanol and acetone environments. These results typically explain that higher polarity of solvents not only affects the lignin linkages (α-O-4 and β-O-4) but also side chains present in the lignin. However, comparison of the yield obtained from experiments with calculated interaction energy of DFT exhibits a small contrast that DFT found a significant difference in interaction energy (around 7 kj mol^{-1}) between lignin-ethanol and lignin-acetone. Whereas, in the case of experiments, a similar yield was observed. It should be noted that the investigated lignin model for DFT calculations is one of the linkages present in the lignin biopolymer and, therefore, the difference is inevitable. Furthermore, another important point to consider is that the trend observed for the solvents used with lignin model can be altered when other lignin linkages or lignin models are examined. Nevertheless, this study provides a rational and fundamental explanation for the predominant interactions that drive the fractionation of lignin using different polarity of solvents.

4. Conclusions

In this work, single-step fractionation of industrial hardwood kraft lignin using organic solvents of different chemical nature was investigated for the first time combining an experimental and theoretical approach. Chemical analyses revealed differences on molecular characteristics in terms of molecular weight distribution and structure of isolated soluble and insoluble fractions. Moreover, principal components analysis (PCA) and partial least squares discriminant analysis (PLS-DA) based on NIR spectroscopy data clearly differentiate samples between soluble and insoluble fractions. Both chemical and chemometric analyses evidenced the special particularity of soluble fraction isolated from diethyl ether, which resulted in homogeneous low molecular mass fraction. We have also employed density functional theory (DFT) calculations to illustrate the underlying mechanism solvents' impact with the lignin model. On the basis of detailed analysis, the results have found that highly polar ethanol solvent strongly interacts with the lignin model more than other examined solvents (acetone, diethyl ether and hexane), and non-polar hexane solvent exhibits the

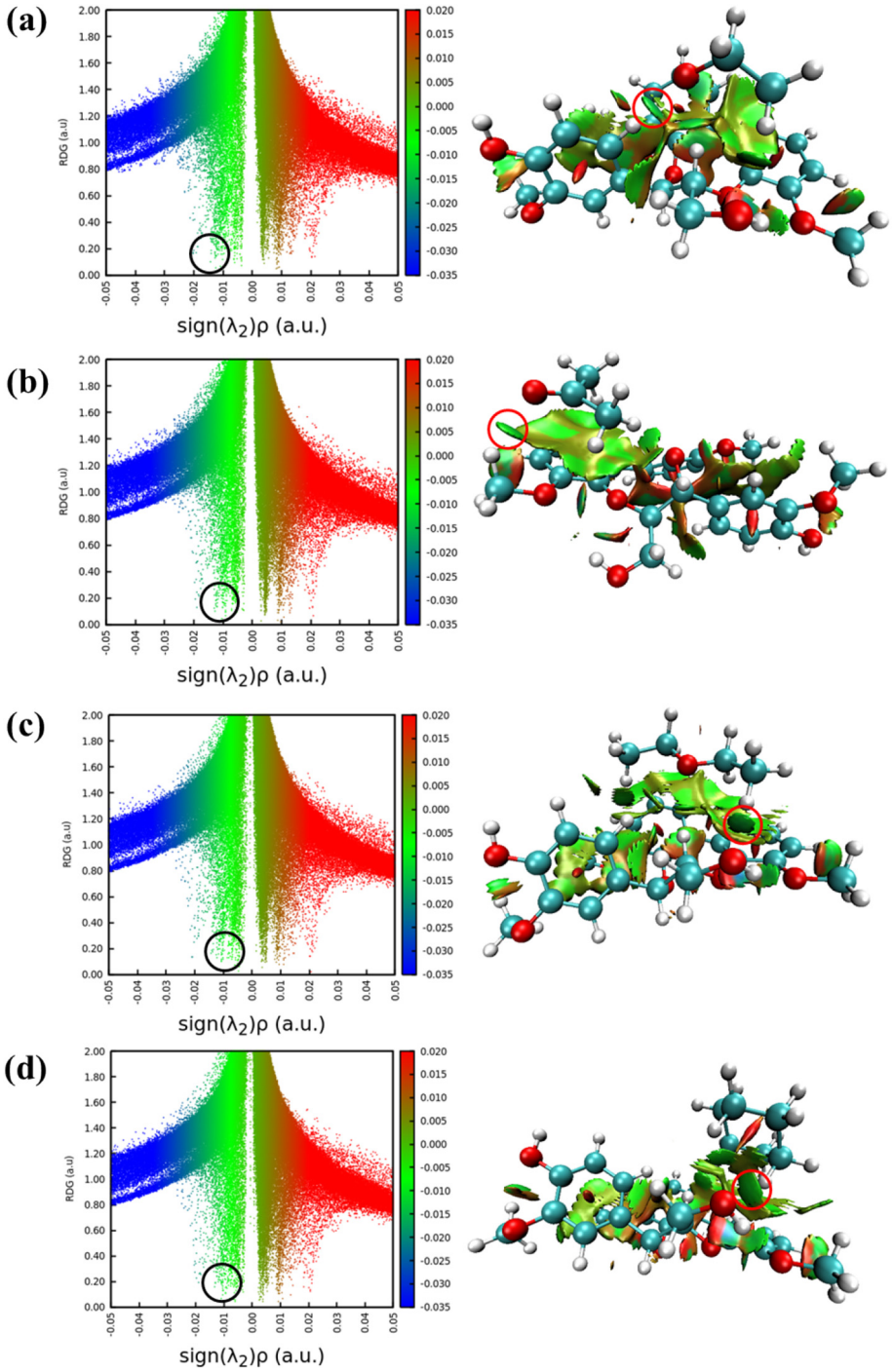

Fig. 8. RDG scatter plots (left) and corresponding non-covalent interaction (NCI) plots (right) of (a) lignin DBD – ethanol, (b) lignin DBD – acetone, (c) lignin DBD – diethyl ether and (d) lignin DBD – hexane. The isosurfaces are colored (right) with respect to the values of sign(λ_2)ρ (a.u.), from −0.03 to 0.02 a.u. Color online: blue represents strong attractive interactions, green indicates van der Waals interactions and red indicates repulsive/steric interactions.

least interaction energy. The different linkages present in the lignin model, α-O and γ-O, undergo a large variation in the bond lengths with ethanol and acetone solvents. Similar trend was also observed for hydrogen bonding and non-covalent interaction analysis, in which ethanol makes the shortest hydrogen bond with lignin model. Aliphatic γ-OH is the prevalent site for strong hydrogen bonds with ethanol, diethyl ether and hexane over aromatic hydroxyl group; however, acetone makes hydrogen bonds with methoxyl group and α-O atom. Chemical reactivity study showed that lignin model with ethanol has a lower band gap than other lignin-solvent, which is evident for high chemical reactivity of the ethanol solvent. This research provides a significant insight and rational explanation about lignin polymer fractionation using organic solvents in order to make it more homogeneous for particular value-added applications.

CRediT authorship contribution statement

Veerapandian Ponnuchamy: Conceptualization, Investigation, Formal analysis, Visualization, Methodology, Visualization, Writing - Original Draft. **Oihana Gordobil:** Conceptualization, Investigation, Formal

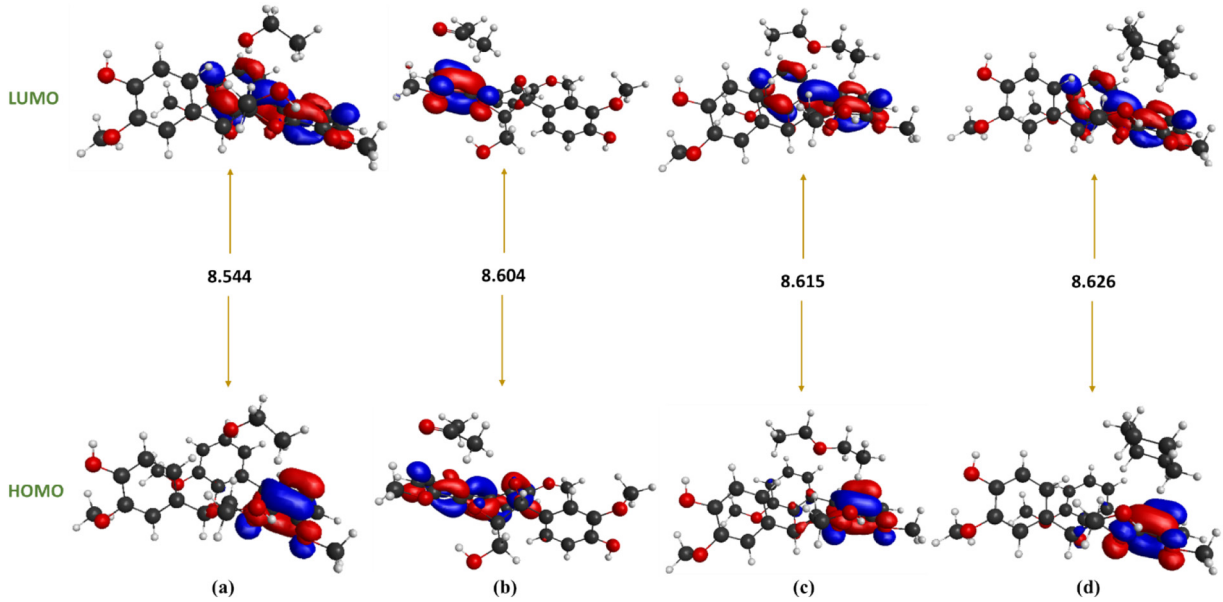

Fig. 9. HOMO-LUMO orbitals with energy band gap (in eV) for lignin-solvent systems (a) lignin DBD – ethanol, (b) lignin DBD – acetone, (c) lignin DBD – diethyl ether and (d) lignin DBD – hexane.

analysis, Visualization, Methodology, Visualization, Writing - Original Draft. **René Herrera Diaz:** Formal analysis, visualization, methodology, writing- Reviewing and Editing. **Anna Sandak:** Writing- Reviewing and Editing. **Jakub Sandak:** Writing- Reviewing and Editing.

Declaration of competing interest

The authors declare that they have no known competing financial interests or personal relationships that could have appeared to influence the work reported in this paper.

Acknowledgement

The authors gratefully acknowledge the European Commission for funding the InnoRenew project [Grant Agreement # 739574] under the Horizon2020 Widespread-Teaming program, the Republic of Slovenia (investment funding from the Republic of Slovenia and the European Union European Regional Development Funds) and infrastructural ARRS program IO-0035. Additionally, O.G. is grateful for the financial support received from the University of the Basque Country (post-doctoral grant DOCREC18/29) and R.H. acknowledges to the Department of Education of the Basque Government (post-doctoral grant INGVTCL4-D00112-7).

Appendix A. Supplementary data

Supplementary data to this article can be found online at https://doi.org/10.1016/j.ijbiomac.2020.11.139.

References

[1] H. Chen, Lignocellulose Biorefinery Engineering: Principles and Applications, Woodhead Publishing, 2015.
[2] R.H. Diaz, L. Bodi-Paul, O. Gordobil, J. Labidi, Fast methods for the identification of suitable chemo-enzymatic treatments of Kraft lignin to obtain aromatic compounds, Biofuels Bioprod. Biorefin. 14 (2020) 521–532, https://doi.org/10.1002/bbb.2093.
[3] M. Österberg, M.H. Sipponen, B.D. Mattos, O.J. Rojas, Spherical lignin particles: a review on their sustainability and applications, Green Chem. 22 (2020) 2712–2733, https://doi.org/10.1039/D0GC00096E.
[4] M.P. Pandey, C.S. Kim, Lignin depolymerization and conversion: a review of thermochemical methods, Chemical Engineering & Technology 34 (2011) 29–41, https://doi.org/10.1002/ceat.201000270.
[5] W. Schutyser, T. Renders, S.V. den Bosch, S.-F. Koelewijn, G.T. Beckham, B.F. Sels, Chemicals from lignin: an interplay of lignocellulose fractionation, depolymerisation, and upgrading, Chem. Soc. Rev. 47 (2018) 852–908, https://doi.org/10.1039/C7CS00566K.
[6] V.K. Thakur, M.K. Thakur, P. Raghavan, M.R. Kessler, Progress in green polymer composites from lignin for multifunctional applications: a review, ACS Sustain. Chem. Eng. 2 (2014) 1072–1092, https://doi.org/10.1021/sc500087z.
[7] A. Naseem, S. Tabasum, K.M. Zia, M. Zuber, M. Ali, A. Noreen, Lignin-derivatives based polymers, blends and composites: a review, Int. J. Biol. Macromol. 93 (2016) 296–313, https://doi.org/10.1016/j.ijbiomac.2016.08.030.
[8] S. Laurichesse, L. Avérous, Chemical modification of lignins: towards biobased polymers, Prog. Polym. Sci. 39 (2014) 1266–1290, https://doi.org/10.1016/j.progpolymsci.2013.11.004.
[9] H. Chung, N.R. Washburn, Chemistry of lignin-based materials, Green Materials 1 (2013) 137–160, https://doi.org/10.1680/gmat.12.00009.
[10] D. Wang, S.H. Lee, J. Kim, C.B. Park, "Waste to wealth": lignin as a renewable building block for energy harvesting/storage and environmental remediation, ChemSusChem 13 (2020) 2807–2827, https://doi.org/10.1002/cssc.202000394.
[11] M. Culebras, G. Ren, S. O'Connell, J.J. Vilatela, M.N. Collins, Lignin doped carbon nanotube yarns for improved thermoelectric efficiency, Advanced Sustainable Systems. n/a (n.d.) 2000147. doi:https://doi.org/10.1002/adsu.202000147.
[12] P. Ortiz-Serna, M. Carsí, M. Culebras, M.N. Collins, M.J. Sanchis, Exploring the role of lignin structure in molecular dynamics of lignin/bio-derived thermoplastic elastomer polyurethane blends, Int. J. Biol. Macromol. 158 (2020) 1369–1379, https://doi.org/10.1016/j.ijbiomac.2020.04.261.
[13] I. Spiridon, P. Poni, G. Ghica, Biological and pharmaceutical applications of lignin and its derivatives: a mini-review, Cellul. Chem. Technol. 52 (2018) 543–550.
[14] S.M. Roopan, An overview of natural renewable bio-polymer lignin towards nano and biotechnological applications, Int. J. Biol. Macromol. 103 (2017) 508–514, https://doi.org/10.1016/j.ijbiomac.2017.05.103.
[15] O. Gordobil, A. Oberemko, G. Saulis, V. Baublys, J. Labidi, In vitro cytotoxicity studies of industrial Eucalyptus kraft lignins on mouse hepatoma, melanoma and Chinese hamster ovary cells, Int. J. Biol. Macromol. 135 (2019) 353–361, https://doi.org/10.1016/j.ijbiomac.2019.05.111.
[16] M.H. Sipponen, H. Lange, C. Crestini, A. Henn, M. Österberg, Lignin for nano- and microscaled carrier systems: applications, trends, and challenges, ChemSusChem 12 (2019) 2039–2054, https://doi.org/10.1002/cssc.201900480.
[17] O. Gordobil, R. Herrera, M. Yahyaoui, S. İlk, M. Kaya, J. Labidi, Potential use of kraft and organosolv lignins as a natural additive for healthcare products, RSC Adv. 8 (2018) 24525–24533, https://doi.org/10.1039/C8RA02255K.
[18] R. Mörck, H. Yoshida, K.P. Kringstad, Fractionation of kraft lignin by successive extraction with organic solvents. I: fonctional groups, 13C-NMR-spectra and molecular weight distributions, Holzforschung 40 (1986) 51–60.
[19] S.Y. Park, J.-Y. Kim, H.J. Youn, J.W. Choi, Fractionation of lignin macromolecules by sequential organic solvents systems and their characterization for further valuable applications, Int. J. Biol. Macromol. 106 (2018) 793–802, https://doi.org/10.1016/j.ijbiomac.2017.08.069.
[20] T.-Q. Yuan, J. He, F. Xu, R.-C. Sun, Fractionation and physico-chemical analysis of degraded lignins from the black liquor of Eucalyptus pellita KP-AQ pulping, Polym. Degrad. Stab. 94 (2009) 1142–1150, https://doi.org/10.1016/j.polymdegradstab.2009.03.019.

[21] X. Jiang, D. Savithri, X. Du, S. Pawar, H. Jameel, H. Chang, X. Zhou, Fractionation and characterization of kraft lignin by sequential precipitation with various organic solvents, ACS Sustain. Chem. Eng. 5 (2017) 835–842, https://doi.org/10.1021/acssuschemeng.6b02174.
[22] A. Duval, F. Vilaplana, C. Crestini, M. Lawoko, Solvent screening for the fractionation of industrial kraft lignin, Holzforschung 70 (2016) 11–20, https://doi.org/10.1515/hf-2014-0346.
[23] G. Wang, T. Pang, Y. Xia, X. Liu, S. Li, A.M. Parvez, F. Kong, C. Si, Subdivision of bamboo kraft lignin by one-step ethanol fractionation to enhance its water-solubility and antibacterial performance, Int. J. Biol. Macromol. 133 (2019) 156–164, https://doi.org/10.1016/j.ijbiomac.2019.04.093.
[24] C. Schuerch, The solvent properties of liquids and their relation to the solubility, swelling, isolation and fractionation of lignin, J. Am. Chem. Soc. 74 (1952) 5061–5067, https://doi.org/10.1021/ja01140a020.
[25] A.P. Dodd, J.F. Kadla, S.K. Straus, Characterization of fractions obtained from two industrial softwood kraft lignins, ACS Sustain. Chem. Eng. 3 (2015) 103–110, https://doi.org/10.1021/sc500601b.
[26] E. Melro, L. Alves, F.E. Antunes, B. Medronho, A brief overview on lignin dissolution, J. Mol. Liq. 265 (2018) 578–584, https://doi.org/10.1016/j.molliq.2018.06.021.
[27] R.W. Thring, M.N. Vanderlaan, S.L. Griffin, Fractionation of Alcell® lignin by sequential solvent extraction, Journal of Wood Chemistry and Technology 16 (1996) 139–154, https://doi.org/10.1080/02773819608545815.
[28] C.G. Boeriu, F.I. Fițigău, R.J.A. Gosselink, A.E. Frissen, J. Stoutjesdijk, F. Peter, Fractionation of five technical lignins by selective extraction in green solvents and characterisation of isolated fractions, Ind. Crop. Prod. 62 (2014) 481–490, https://doi.org/10.1016/j.indcrop.2014.09.019.
[29] C. Allegretti, S. Fontanay, K. Rischka, A. Strini, J. Troquet, S. Turri, G. Griffini, P. D'Arrigo, Two-step fractionation of a model technical lignin by combined organic solvent extraction and membrane ultrafiltration, ACS Omega 4 (2019) 4615–4626, https://doi.org/10.1021/acsomega.8b02851.
[30] V. Passoni, C. Scarica, M. Levi, S. Turri, G. Griffini, Fractionation of industrial softwood kraft lignin: solvent selection as a tool for tailored material properties, ACS Sustain. Chem. Eng. 4 (2016) 2232–2242, https://doi.org/10.1021/acssuschemeng.5b01722.
[31] A. Beste, A.C. Buchanan, Role of carbon–carbon phenyl migration in the pyrolysis mechanism of β-O-4 lignin model compounds: phenethyl phenyl ether and α-hydroxy phenethyl phenyl ether, J. Phys. Chem. A 116 (2012) 12242–12248, https://doi.org/10.1021/jp3104694.
[32] N. Sun, R. Parthasarathi, A.M. Socha, J. Shi, S. Zhang, V. Stavila, K.L. Sale, B.A. Simmons, S. Singh, Understanding pretreatment efficacy of four cholinium and imidazolium ionic liquids by chemistry and computation, Green Chem. 16 (2014) 2546–2557, https://doi.org/10.1039/C3GC42401D.
[33] A. Beste, A.C. Buchanan, Computational investigation of the pyrolysis product selectivity for α-hydroxy phenethyl phenyl ether and phenethyl phenyl ether: analysis of substituent effects and reactant conformer selection, J. Phys. Chem. A 117 (2013) 3235–3242, https://doi.org/10.1021/jp4015004.
[34] W. Ji, Z. Ding, J. Liu, Q. Song, X. Xia, H. Gao, H. Wang, W. Gu, Mechanism of lignin dissolution and regeneration in ionic liquid, Energy Fuel 26 (2012) 6393–6403, https://doi.org/10.1021/ef301231a.
[35] Y. Zhang, H. He, K. Dong, M. Fan, S. Zhang, A DFT study on lignin dissolution in imidazolium-based ionic liquids, RSC Adv. 7 (2017) 12670–12681, https://doi.org/10.1039/C6RA27059J.
[36] H. Ji, P. Lv, Mechanistic insights into the lignin dissolution behaviors of a recyclable acid hydrotrope, deep eutectic solvent (DES), and ionic liquid (IL), Green Chem. 22 (2020) 1378–1387, https://doi.org/10.1039/C9GC02760B.
[37] T. Elder, Bond dissociation enthalpies of a dibenzodioxocin lignin model compound, Energy Fuel 27 (2013) 4785–4790, https://doi.org/10.1021/ef401026g.
[38] T. Elder, Bond dissociation enthalpies of a pinoresinol lignin model compound, Energy Fuel 28 (2014) 1175–1182, https://doi.org/10.1021/ef402310h.
[39] L. Chen, X. Wang, H. Yang, Q. Lu, D. Li, Q. Yang, H. Chen, Study on pyrolysis behaviors of non-woody lignins with TG-FTIR and Py-GC/MS, J. Anal. Appl. Pyrolysis 113 (2015) 499–507, https://doi.org/10.1016/J.JAAP.2015.03.018.
[40] H. Li, A.G. McDonald, Fractionation and characterization of industrial lignins, Ind. Crop. Prod. 62 (2014) 67–76, https://doi.org/10.1016/j.indcrop.2014.08.013.
[41] J. Fernández-Rodríguez, X. Erdocia, C. Sánchez, M. González Alriols, J. Labidi, Lignin depolymerization for phenolic monomers production by sustainable processes, Journal of Energy Chemistry 26 (2017) 622–631, https://doi.org/10.1016/j.jechem.2017.02.007.
[42] Y. Zhu, J. Yan, C. Liu, D. Zhang, Modeling interactions between a β-O-4 type lignin model compound and 1-allyl-3-methylimidazolium chloride ionic liquid, Biopolymers 107 (2017), e23022, https://doi.org/10.1002/bip.23022.
[43] F. Mostaghni, A. Teimouri, S.A. Mirshokraei, Synthesis, spectroscopic characterization and DFT calculations of β-O-4 type lignin model compounds, Spectrochim. Acta A Mol. Biomol. Spectrosc. 110 (2013) 430–436, https://doi.org/10.1016/j.saa.2013.03.075.
[44] Y. Zhu, Z. Han, L. Fu, C. Liu, D. Zhang, Cleavage of the β–O–4 bond in a lignin model compound using the acidic ionic liquid 1-H^{-3}-methylimidazolium chloride as catalyst: a DFT mechanistic study, J. Mol. Model. 24 (2018) 322, https://doi.org/10.1007/s00894-018-3854-x.
[45] M.W. Schmidt, K.K. Baldridge, J.A. Boatz, S.T. Elbert, M.S. Gordon, J.H. Jensen, S. Koseki, N. Matsunaga, K.A. Nguyen, S. Su, T.L. Windus, M. Dupuis, J.A. Montgomery, General atomic and molecular electronic structure system, J. Comput. Chem. 14 (1993) 1347–1363, https://doi.org/10.1002/jcc.540141112.
[46] J.D. Kubicki, M.N.-A. Mohamed, H.D. Watts, Quantum mechanical modeling of the structures, energetics and spectral properties of Iα and Iβ cellulose, Cellulose 20 (2013) 9–23, https://doi.org/10.1007/s10570-012-9838-6.
[47] M. Cirtog, M.E. Alikhani, B. Madebène, P. Soulard, P. Asselin, B. Tremblay, Bonding nature and vibrational signatures of oxirane:(water)n=1–3. Assessment of the performance of the dispersion-corrected DFT methods compared to the ab initio results and Fourier transform infrared experimental data, J. Phys. Chem. A 115 (2011) 6688–6701, https://doi.org/10.1021/jp202867t.
[48] A.V. Marenich, C.J. Cramer, D.G. Truhlar, Universal solvation model based on solute electron density and on a continuum model of the solvent defined by the bulk dielectric constant and atomic surface tensions, J. Phys. Chem. B 113 (2009) 6378–6396, https://doi.org/10.1021/jp810292n.
[49] Jmol: an open-source Java viewer for chemical structures in 3D, http://www.jmol.org/ ((accessed June 29, 2020), (n.d.). http://jmol.sourceforge.net/ (accessed June 26, 2020)).
[50] B.M. Bode, M.S. Gordon, Macmolplt: a graphical user interface for GAMESS, J. Mol. Graph. Model. 16 (1998) 133–138, https://doi.org/10.1016/S1093-3263(99)00002-9.
[51] R.F.W. Bader, Atoms in molecules, Acc. Chem. Res. 18 (1985) 9–15, https://doi.org/10.1021/ar00109a003.
[52] S.J. Grabowski, Non-covalent interactions – QTAIM and NBO analysis, J. Mol. Model. 19 (2013) 4713–4721, https://doi.org/10.1007/s00894-012-1463-7.
[53] J. Contreras-García, E.R. Johnson, S. Keinan, R. Chaudret, J.-P. Piquemal, D.N. Beratan, W. Yang, NCIPLOT: a program for plotting noncovalent interaction regions, J. Chem. Theory Comput. 7 (2011) 625–632, https://doi.org/10.1021/ct100641a.
[54] E.R. Johnson, S. Keinan, P. Mori-Sánchez, J. Contreras-García, A.J. Cohen, W. Yang, Revealing noncovalent interactions, J. Am. Chem. Soc. 132 (2010) 6498–6506, https://doi.org/10.1021/ja100936w.
[55] C.M. Breneman, K.B. Wiberg, Determining atom-centered monopoles from molecular electrostatic potentials. The need for high sampling density in formamide conformational analysis, J. Comput. Chem. 11 (1990) 361–373, https://doi.org/10.1002/jcc.540110311.
[56] G. Schaftenaar, J.H. Noordik, Molden: a pre- and post-processing program for molecular and electronic structures, J. Comput. Aided Mol. Des. 14 (2000) 123–134, https://doi.org/10.1023/A:1008193805436.
[57] T. Lu, F. Chen, Multiwfn: a multifunctional wavefunction analyzer, J. Comput. Chem. 33 (2012) 580–592, https://doi.org/10.1002/jcc.22885.
[58] J.L. Espinoza-Acosta, P.I. Torres-Chávez, B. Ramírez-Wong, C.M. López-Saiz, B. Montaño-Leyva, Antioxidant, antimicrobial, and antimutagenic properties of technical lignins and their applications, BioResources 11 (2016) 5452–5481.
[59] O. Gordobil, R. Moriana, L. Zhang, J. Labidi, O. Sevastyanova, Assesment of technical lignins for uses in biofuels and biomaterials: structure-related properties, proximate analysis and chemical modification, Ind. Crop. Prod. 83 (2016) 155–165, https://doi.org/10.1016/j.indcrop.2015.12.048.
[60] H. Sadeghifar, D.S. Argyropoulos, Macroscopic behavior of kraft lignin fractions: melt stability considerations for lignin–polyethylene blends, ACS Sustain. Chem. Eng. 4 (2016) 5160–5166, https://doi.org/10.1021/acssuschemeng.6b00636.
[61] K. Wang, F. Xu, R. Sun, Molecular characteristics of kraft-AQ pulping lignin fractionated by sequential organic solvent extraction, Int. J. Mol. Sci. 11 (2010) 2988–3001, https://doi.org/10.3390/ijms11082988.
[62] Y. Deng, X. Feng, M. Zhou, Y. Qian, H. Yu, X. Qiu, Investigation of aggregation and assembly of alkali lignin using iodine as a probe, Biomacromolecules 12 (2011) 1116–1125, https://doi.org/10.1021/bm101449b.
[63] J. Domínguez-Robles, T. Tamminen, T. Liitiä, M.S. Peresin, A. Rodríguez, A.-S. Jääskeläinen, Aqueous acetone fractionation of kraft, organosolv and soda lignins, Int. J. Biol. Macromol. 106 (2018) 979–987, https://doi.org/10.1016/j.ijbiomac.2017.08.102.
[64] S. Wang, B. Ru, H. Lin, W. Sun, Z. Luo, Pyrolysis behaviors of four lignin polymers isolated from the same pine wood, Bioresour. Technol. 182 (2015) 120–127, https://doi.org/10.1016/j.biortech.2015.01.127.
[65] M. Zhang, F.L.P. Resende, A. Moutsoglou, D.E. Raynie, Pyrolysis of lignin extracted from prairie cordgrass, aspen, and kraft lignin by Py-GC/MS and TGA/FTIR, J. Anal. Appl. Pyrolysis 98 (2012) 65–71, https://doi.org/10.1016/j.jaap.2012.05.009.
[66] S. Constant, H.L.J. Wienk, A.E. Frissen, P. de Peinder, R. Boelens, D.S. van Es, R.J.H. Grisel, B.M. Weckhuysen, W.J.J. Huijgen, R.J.A. Gosselink, P.C.A. Bruijnincx, New insights into the structure and composition of technical lignins: a comparative characterisation study, Green Chem. 18 (2016) 2651–2665, https://doi.org/10.1039/C5GC03043A.
[67] J.S. Kim, Y.Y. Lee, T.H. Kim, A review on alkaline pretreatment technology for bioconversion of lignocellulosic biomass, Bioresour. Technol. 199 (2016) 42–48, https://doi.org/10.1016/j.biortech.2015.08.085.
[68] D. Tarasov, M. Leitch, P. Fatehi, Lignin–carbohydrate complexes: properties, applications, analyses, and methods of extraction: a review, Biotechnology for Biofuels 11 (2018) 269, https://doi.org/10.1186/s13068-018-1262-1.
[69] R.J.A. Gosselink, J.E.G. van Dam, E. de Jong, E.L. Scott, J.P.M. Sanders, J. Li, G. Gellerstedt, Fractionation, analysis, and PCA modeling of properties of four technical lignins for prediction of their application potential in binders, Holzforschung 64 (2010) 193–200, https://doi.org/10.1515/hf.2010.023.
[70] Z. Ma, Q. Sun, J. Ye, Q. Yao, C. Zhao, Study on the thermal degradation behaviors and kinetics of alkali lignin for production of phenolic-rich bio-oil using TGA–FTIR and Py–GC/MS, J. Anal. Appl. Pyrolysis 117 (2016) 116–124, https://doi.org/10.1016/j.jaap.2015.12.007.
[71] I. Dávila, P. Gullón, M.A. Andrés, J. Labidi, Coproduction of lignin and glucose from vine shoots by eco-friendly strategies: toward the development of an integrated biorefinery, Bioresour. Technol. 244 (2017) 328–337, https://doi.org/10.1016/j.biortech.2017.07.104.
[72] J. Ponomarenko, T. Dizhbite, M. Lauberts, A. Viksna, G. Dobele, O. Bikovens, G. Telysheva, Characterization of softwood and hardwood lignoboost kraft lignins

with emphasis on their antioxidant activity, BioResources 9 (2014) 2051–2068, https://doi.org/10.15376/biores.9.2.2051-2068.
[73] J. Ponomarenko, T. Dizhbite, M. Lauberts, A. Volperts, G. Dobele, G. Telysheva, Analytical pyrolysis - a tool for revealing of lignin structure-antioxidant activity relationship, J. Anal. Appl. Pyrolysis 113 (2015) 360–369, https://doi.org/10.1016/j.jaap.2015.02.027.
[74] M. Schwanninger, J.C. Rodrigues, K. Fackler, A review of band assignments in near infrared spectra of wood and wood components, J. Near Infrared Spectrosc. 19 (2011) 287–308.
[75] R.G. Parr, Density functional theory of atoms and molecules, in: K. Fukui, B. Pullman (Eds.), Horizons of Quantum Chemistry, Springer Netherlands, Dordrecht 1980, pp. 5–15, https://doi.org/10.1007/978-94-009-9027-2_2.
[76] I. Fleming, Frontier Orbitals and Organic Chemical Reactions, Wiley, 1976.
[77] Q. Xia, Y. Liu, J. Meng, W. Cheng, W. Chen, S. Liu, Y. Liu, J. Li, H. Yu, Multiple hydrogen bond coordination in three-constituent deep eutectic solvents enhances lignin fractionation from biomass, Green Chem. 20 (2018) 2711–2721, https://doi.org/10.1039/C8GC00900G.
[78] J. Shi, S. Pattathil, R. Parthasarathi, N.A. Anderson, J.I. Kim, S. Venketachalam, M.G. Hahn, C. Chapple, B.A. Simmons, S. Singh, Impact of engineered lignin composition on biomass recalcitrance and ionic liquid pretreatment efficiency, Green Chem. 18 (2016) 4884–4895, https://doi.org/10.1039/C6GC01193D.
[79] D.V. Wagle, C.A. Deakyne, G.A. Baker, Quantum chemical insight into the interactions and thermodynamics present in choline chloride based deep eutectic solvents, J. Phys. Chem. B 120 (2016) 6739–6746, https://doi.org/10.1021/acs.jpcb.6b04750.
[80] H. Li, Y. Chang, W. Zhu, C. Wang, C. Wang, S. Yin, M. Zhang, H. Li, Theoretical evidence of charge transfer interaction between SO2 and deep eutectic solvents formed by choline chloride and glycerol, Phys. Chem. Chem. Phys. 17 (2015) 28729–28742, https://doi.org/10.1039/C5CP04172D.